Structural Studies on Single Crystals of Chevrel Phase Selenides $REMo_6Se_8$ (RE = La, Ce, Pr, Nd, or Sm) at 298 K

F. Le Berre,*,† C. Hamard,† O. Peña,† and A. Wojakowski‡

Laboratoire de Chimie du Solide et Inorganique Moléculaire, LCSIM-UMR 6511, Université de Rennes I, 35042 Rennes Cedex, France, and Institute of Low Temperature and Structure Research, Polish Academy of Sciences, 50950 Wroclaw, Poland

Received June 30, 1999

We report on structural studies at room temperature of rare-earth based Chevrel phase selenides of the formula $RE_xMo_6Se_8$, where RE stands for a light rare-earth La (**1**), Ce (**2**), Pr (**3**), Nd (**4**), or Sm (**5**). The single crystals were grown at 1650 °C < T < 1690 °C from off-stoichiometric starting compositions, with the exception of **3**, which was grown at 1710 °C from a stoichiometric charge (congruently melting material). The crystal structures were solved in space group $R\bar{3}$ (No. 148; $Z = 1$) and found to be isostructural with the well-known Chevrel phases having large cations (e.g., $PbMo_6S_8$, $REMo_6S_8$). The structures are based on Mo_6Se_8 metallic clusters that are slightly rotated inside a pseudocubic rare-earth sublattice. Structural refinements revealed that the origin site, occupied by the RE atoms, exhibits slight deficiencies, leading to a $RE_xMo_6Se_8$ composition, with x ranging between ∼0.82 and ∼0.92: **1** $La_{0.88}Mo_6Se_8$, $a_{rh} = 6.7577(9)$ Å, $\alpha_{rh} = 88.62(2)°$; **2a** $Ce_{0.82}Mo_6Se_8$, $a_{rh} = 6.7407(6)$ Å, $\alpha_{rh} = 88.83(2)°$; **2b** $Ce_{0.92}Mo_6Se_8$, $a_{rh} = 6.7473(9)$ Å, $\alpha_{rh} = 88.69(2)°$; **3** $Pr_{0.86}Mo_6Se_8$, $a_{rh} = 6.7385(6)$ Å, $\alpha_{rh} = 88.81(2)°$; **4** $Nd_{0.85}Mo_6Se_8$, $a_{rh} = 6.7286(5)$ Å, $\alpha_{rh} = 88.85(1)°$; and **5** $Sm_{0.87}Mo_6Se_8$, $a_{rh} = 6.7182(2)$ Å, $\alpha_{rh} = 88.956(3)°$. All of the structural data presented in this work (lattice constants, positionnal parameters and interatomic distances) concern an average RE content of $x \approx 0.87$. In this way, any influence due to electronic effects (VEC number) can be discarded, and exact correlations between these parameters and the ionic radius of the rare-earth atoms can then be established.

(1) Introduction

The coexistence of superconductivity and long-range magnetic order has been a long-standing problem in solid-state physics. The discovery of Chevrel phases, $M_xMo_6X_8$ (M = transition metal, rare earth (RE), etc; X = chalcogen), in 1971 brought up a completely new situation.[1] Indeed, compounds based on a rare-earth cation, $REMo_6X_8$, showed for the first time that a system containing a regular lattice of magnetic atoms could be superconductive. With the exception of RE = Ce and Eu, all ternary compounds of the $REMo_6S_8$ and $REMo_6Se_8$ types are superconductors, with T_c varying from 1.5 K to 7 K for the first series and from 5.5 K to 11 K for the selenides (N.B. that magnetic order may occur at ∼0.5−2 K for RE = Gd, Er, Ho, etc...).[2]

Obviously, studying single crystals constitutes the best way to determine the structural and physical properties of any material. However, in the case of the $REMo_6X_8$ compounds, a major obstacle to crystal growth concerns the peritectic character of their melting.[3] In addition, their high melting points,[3,4] together with their high chemical reactivity and their sensitivity to oxidation, make the crystal growth of these materials very complex. These problems have been difficult to solve and have long delayed any progress in the crystal growth of Chevrel-phase $REMo_6X_8$ compounds. Several works performed in the mid-1980s successfully led to the crystallization of the sulfide series $REMo_6S_8$ (see refs 4 and 5), thus allowing the study of their structural and physical properties. Concerning the selenide series, however, technical problems related to the high toxicity of selenide vapors impose far more precautions. In addition, the existence of a stable binary-phase Mo_6Se_8, isostructural to $REMo_6Se_8$, makes crystals of the ternary compound more difficult to obtain. The first trials, performed by the same research group, led to biphased crystals with cocrystallization of Mo_6Se_8 and $REMo_6Se_8$, both phases growing simultaneously.[6] Thus, a different approach from the one applied for sulfides was necessary to obtain $REMo_6Se_8$ crystals. This new method primarily consisted of a 24 h presintering of off-stoichiometric compositions followed by melting them at high temperatures. The melt is then slowly cooled, yielding single crystals of the $REMo_6Se_8$ phase.

In this work, we report for the first time full results on the crystal structure of several $REMo_6Se_8$ compounds containing light rare-earth atoms (La, Ce, Pr, Nd, and Sm). From this study, thorough correlations between structural parameters and the rare-earth, ionic size can be established, showing in particular the importance of steric effects on the interatomic distances. Stoichiometry effects in the $La_xMo_6Se_8$ phase and original structural features in the $EuMo_6Se_8$ phase have been

* Present address: Laboratoire des Fluorures, UPRES A 6010, Université du Maine, 72017 Le Mans, France. Phone: (33) 02 43 83 33 46. Fax: (33) 02 43 83 35 06. E-mail: le_berre@fluo.univ-lemans.fr.

† Université de Rennes I.

‡ Polish Academy of Sciences.

(1) Chevrel, R.; Sergent, M.; Prigent J. *J. Solid State Chem.* **1971**, *3*, 515.
(2) Fischer, Ø. *Appl. Phys.* **1978**, *16*, 1.
(3) Flukiger, R. In *Superconductor Materials Science*; Foner, S., Schwartz, B., Eds.; Series B; Plenum: New York, 1981; pp 511−604.
(4) Horyn, R.; Peña, O.; Geantet, C.; Sergent, M. *Supercond. Sci. Technol.* **1989**, *2*, 71.
(5) Peña, O.; Sergent, M. *Prog. Solid State Chem.* **1989**, *19*, 165.
(6) Horyn, R.; Peña, O.; Wojakowski, A.; Sergent, M. *Supercond. Sci. Technol.* **1994**, *7*, 146.

10.1021/ic990762z CCC: $19.00
Published on Web 02/26/2000

Table 1. Starting Composition and Estimated Melting Temperature of $RE_xMo_6Se_8$ Compounds

compd	starting composition	melting T (°C)[10,18]
1: $LaMo_6Se_8$	$La_{15}Mo_{32}Se_{53}$	1675
2: $CeMo_6Se_8$	$Ce_{15}Mo_{30}Se_{55}$	1675
3: $PrMo_6Se_8$	$Pr_{6.66}Mo_{40}Se_{53.33}$	1710
4: $NdMo_6Se_8$	$Nd_{17.06}Mo_{27.29}Se_{55.65}$	1650
5: $SmMo_6Se_8$	$Sm_{15}Mo_{30}Se_{55}$	1685

presented elsewhere.[7,8] The single crystal physical characterization (magnetic, electrical, and superconducting properties) of the compounds presented in this work has been thoroughly discussed in ref 9.

(2) Materials Elaboration

Chevrel phases are produced by solid-state reactions of starting materials such as $MoSe_2$, molybdenum metal, and a rare-earth selenide, all in powder form. $MoSe_2$ is prepared by direct synthesis using Mo powder (Plansee, purity 99.99%), after reduction under a hydrogen gas flow at 850 °C for 4 h. The rare-earth selenides are obtained by direct reaction between the metal (La, Johnson Matthey, 3 N; Ce, Strem Chem., 3 N; Pr, Strem Chem., 3 N; Nd, Strem Chem., 3 N; Sm, Strem Chem., 3 N) and the chalcogen (Fluka, 4 N5). The reaction is performed in a silica tube, with the metallic pieces placed in an alumina boat in order to avoid direct contact between the metal and the silica. The tube is then sealed under secondary vacuum and slowly heated to 950 °C, until the selenide is totally consumed. The exact stoichiometry of $RESe_y$ can be determined by burning a part of the final product in open air and transforming it into the corresponding oxide.

Mixtures of appropriate proportions of the starting materials are prepared and pressed into pellets. These pellets are placed inside a molybdenum crucible, which is previously outgassed in a high-frequency furnace under secondary vacuum. The crucibles are then sealed by arc-melting techniques and placed in a graphite-resistor furnace regulated by an optical pyrometer. During the thermal cycle, a normal-pressure argon flow is kept through the furnace. After presintering for 24 h at 1200 °C, the crystal growth occurs following a well-defined temperature profile based mainly on a rapid increase of temperature up to the melting point followed by a slow cooling. Several trials are necessary to determine the optimum starting composition and melting temperature of each phase. For RE = La, Ce, Nd, and Sm, the best starting composition corresponds, approximately, to $RE_{15}Mo_{30}Se_{55}$ (Table 1). In the case of $NdMo_6Se_8$, the slightly different composition is due to the stoichiometry of the available neodymium selenide. A special case among this series concerns the praseodymium compound $PrMo_6Se_8$ (**3**), for which a nominal composition $Pr_{6.66}Mo_{40}Se_{53.33}$ corresponding to the exact stoichiometry ⟨1:6:8⟩ of the ternary phase gave the best crystals.[10] This result suggests that $PrMo_6Se_8$, together with $EuMo_6Se_8$,[8] is rather congruently melting, unlike the other members of the series. This fact can explain the higher melting temperatures observed for these two compounds (1710 °C and 1720 °C, respectively), compared to noncongruent melting systems (Table 1). Similar behavior was observed in the sulfides $REMo_6S_8$, in which the melting temperatures of $EuMo_6S_8$ and $YbMo_6S_8$, two congruently melting compounds, were systematically higher than those of the rest of the series.[5]

The final product obtained after melting primarily consists of a mixture of crystals of the desired ternary phase imbedded in a rare-earth selenide crust. The latter is dissolved in a solution of ethyl alcohol and hydrochloric acid. The $REMo_6Se_8$ single crystals are then collected, selected under an optical microscope, and cleaned with alcohol in ultrasonic bath. Some of them are used, after being crushed, to perform X-ray powder diffraction analysis in order to check the quality of the crystals. The resulting powder diffraction pattern corresponds to the expected Chevrel-phase crystal structure. Additional analysis by EDX/SEM techniques confirm the good quality of the single crystals.

At this point, for completeness, we should remark that all our efforts using these or other methods to produce single crystals of heavy rare-earth materials of the $REMo_6Se_8$ type (RE: Gd → Yb) have been completely unsuccessful until now, all trials ending with biphased crystals formed by alternate layers of Mo_6Se_8 and $REMo_6Se_8$. Very recent HREM investigations at the interface[11] reveal, in fact, that cocrystallization occurs when lattice parameters of the binary and ternary phases become very close, as it occurs for the second half of the series. As we shall discuss later in this work, the increasing rare-earth ionic radius when going from Sm to La will keep the corresponding parameters away from each other, and epitaxial growth will be avoided, allowing good-quality single crystals to be grown.

We should finally remark that all crystals, with the exception of $CeMo_6Se_8$, were found to be superconducting with Tc, measured by an inductive method (i.e., ac susceptibility) ranging from 7.1 K ($SmMo_6Se_8$) up to 11.1 K ($LaMo_6Se_8$).

(3) Instrumental Setup and Structural Refinement

The intensities were recorded at room temperature with an automatic X-ray ENRAF-NONIUS CAD-4 four-circle diffractometer using graphite-monochromated Mo Kα radiation (λ = 0.71069 Å). A $\omega-2\Theta$ scan technique was applied in half the reciprocal space ($\Theta < 45°$). Three standard reflections were monitored every 60 min with no intensity decay. The intensities were corrected for the Lorentz-polarization factor.

All calculations were performed using the MolEN program implemented on a Microvax minicomputer. One absorption correction was applied depending on the size and the form of the crystal (Gaussian correction,[12] spherical or Ψ-scan corrections[13]).

The crystal structure was refined in space group $R\bar{3}$ (No. 148; $Z = 1$), assuming that it was isotypic with those corresponding to Chevrel-phase structures with large cations, such as $PbMo_6S_8$[14] or $REMo_6S_8$:[15] the molybdenum (Mo) and selenium (Se_1) atoms were placed in position 6*f*, Se_2 was placed in position 2*c*, and the rare-earth atom was fixed at the site 1*a*. All of these positions were first assumed to be fully occupied. Occupancies of all sites were equal to unity, except those for the rare-earth site at which significant electron deficiencies were observed. This feature was observed for every crystal that was tested in this work. To make reliable correlations, several crystals were studied for each phase until crystals presenting approximately the same stoichiometry were found. This stoichiometry corresponded to the formula

(7) Le Berre, F.; Peña, O.; Perrin, C.; Sergent, M.; Horyn, R.; Wojakowski, A. *J. Solid State Chem.* **1998**, *136*, 151.
(8) Le Berre, F.; Peña, O.; Perrin, C.; Padiou, J.; Horyn, R.; Wojakowski, A. *J. Alloys Compd.* **1998**, *280*, 85.
(9) Le Berre, F.; Peña, O.; Hamard, C.; Horyn, R.; Wojakowski, A. *J. Alloys Compd.* **1997**, *262−263*, 406.
(10) Hamard, C. Thesis, University of Rennes I, France, 1999. Hamard, C.; Wojakowski, A.; Peña, O. To be published.
(11) Hamard, C.; Lancin, M.; Marhic, C.; Peña, O. To be published.
(12) Coppeno, P.; Leiserowitz, L.; Rabinovich, D. *Acta Crystallogr*. **1965**, *18*, 1035.
(13) Fair, C. K. *MolEN, An Interactive Intelligent System for Crystal Structure Analysis*; Enraf Nonius: Delft, The Netherlands, 1990.

Table 2. Crystal Data and Experimental Parameters Determined from the Single Crystal X-ray Data Collection

compd	**1**	**2a**	**2b**	**3**	**4**	**5**
formula	$La_{0.88}Mo_6Se_8$	$Ce_{0.82}Mo_6Se_8$	$Ce_{0.92}Mo_6Se_8$	$Pr_{0.86}Mo_6Se_8$	$Nd_{0.85}Mo_6Se_8$	$Sm_{0.87}Mo_6Se_8$
fw	1329.60	1322.22	1336.83	1325.62	1329.56	1338.03
space grp	$R\bar{3}$	$R\bar{3}$	$R\bar{3}$	$R\bar{3}$	$R\bar{3}$	$R\bar{3}$
a_{rh} (Å)	6.7577(9)	6.7407(6)	6.7473(9)	6.7385(6)	6.7286(5)	6.7182(2)
α_{rh} (deg)	88.62(2)	88.83(2)	88.69(2)	88.81(2)	88.85(1)	88.956(3)
V_{rh} (Å^3)	308.2(2)	306.1(1)	306.9(1)	305.8(2)	304.4(1)	303.06(3)
ρ_{calcd} (g·cm^{-3})	7.16	7.17	7.23	7.20	7.25	7.33
μ (Mo Kα) (cm^{-1})	3.25	3.30	3.29	3.33	3.37	3.44
R^a	0.039	0.039	0.028	0.032	0.036	0.045
$R_w{}^b$	0.051	0.051	0.037	0.051	0.046	0.056

^{a} $R = \sum(|F_o| - (|F_c|)$. ^{b} $R_w = \sum w(|F_o| - (|F_c|)^2$ with $w = 4F_o{}^2/[\sigma^2 F_o{}^2 + (0.06F_o{}^2)^2]$

Table 3. Positional Parameters, Site Multiplicities, Atomic Occupancy, and Equivalent Isotropic *B* Factors for the Four Independent Atoms and Their Estimated Standard Deviations ($B_{eq} = (4/3)\Sigma\Sigma\beta_{ij}a_ia_j$)

	atom	position	atomic occupancy	*x*	*y*	*z*	B_{eq} (Å^2)
1: $La_{0.88}Mo_6Se_8$	La	1*a*	0.882(2)	0	0	0	0.921(2)
	Mo	6*f*	1	0.23535(4)	0.42250(4)	0.56163(4)	0.437(3)
	Se(1)	6*f*	1	0.37848(5)	0.12040(5)	0.75313(5)	0.608(4)
	Se(2)	2*c*	1	0.24212(5)	0.2421	0.2421	0.674(2)
2a: $Ce_{0.82}Mo_6Se_8$	Ce	1*a*	0.814(2)	0	0	0	1.000(3)
	Mo	6*f*	1	0.43926(5)	0.76595(5)	0.57762(5)	0.486(4)
	Se(1)	6*f*	1	0.37730(7)	0.12086(6)	0.75401(7)	0.654(5)
	Se(2)	2*c*	1	0.75958(7)	0.760	0.760	0.734(2)
2b: $Ce_{0.92}Mo_6Se_8$	Ce	1*a*	0.924(2)	0	0	0	0.932(2)
	Mo	6*f*	1	0.57726(4)	0.43857(4)	0.76539(4)	0.412(3)
	Se(1)	6*f*	1	0.12069(5)	0.75443(5)	0.37699(5)	0.576(4)
	Se(2)	2*c*	1	0.24139(5)	0.241	0.241	0.637(2)
3: $Pr_{0.86}Mo_6Se_8$	Pr	1*a*	0.861(2)	0	0	0	0.927(3)
	Mo	6*f*	1	0.56078(5)	0.23381(5)	0.42270(5)	0.390(5)
	Se(1)	6*f*	1	0.75492(7)	0.37620(7)	0.12105(7)	0.559(6)
	Se(2)	2*c*	1	0.75991(7)	0.760	0.760	0.609(3)
4: $Nd_{0.85}Mo_6Se_8$	Nd	1*a*	0.847(2)	0	0	0	0.951(3)
	Mo	6*f*	1	0.56031(6)	0.2333(6)	0.42264(6)	0.356(5)
	Se(1)	6*f*	1	0.75331(7)	0.37547(8)	0.12132(7)	0.526(6)
	Se(2)	2*c*	1	0.76071(7)	0.761	0.761	0.601(3)
5: $Sm_{0.87}Mo_6Se_8$	Sm	1*a*	0.871(2)	0	0	0	1.002(3)
	Mo	6*f*	1	0.23259(7)	0.42285(7)	0.55977(7)	0.348(5)
	Se(1)	6*f*	1	0.37394(9)	0.12178(9)	0.75603(9)	0.513(7)
	Se(2)	2*c*	1	0.76172(9)	0.762	0.762	0.542(3)

$RE_xMo_6Se_8$, with $x \approx 0.87$. After a further and final refinement, no residual peak was observed.

Selected crystallographic data are given in Table 2, and the rare-earth occupancies, the positional parameters, and the equivalent isotropic *B* factors are given in Table 3.

(4) Crystal Structure

Figure 1 represents the crystal structure of Chevrel phases with large cations. The $REMo_6X_8$ compounds can be described as a stacking of Mo_6X_8 units. These units are slightly distorted cubes with the chalcogen atoms at the corners. The Mo atoms, located at the center of the faces of these cubes, form a distorted octahedron cluster. Consequently, two characteristic distances in the Mo_6 cluster exist: $(Mo-Mo)_\Delta{}^{intra}$ between atoms located on the same plane perpendicular to the ternary axis and $(Mo_\Delta-Mo_\Delta)^{intra}$ between atoms situated on two neighboring planes.

The corner of each Mo_6X_8 cube lies directly opposite to the center of one of the faces of an adjacent cube, which means that there are close contacts between the Mo atoms and the chalcogen atoms of nearby units. Thus, each molybdenum atom is bonded to one Se_2 that is situated on the ternary axis ($(Mo-Se_2)$) and to four Se_1 atoms, one of which belonging to an adjacent Mo_6Se_8 unit ($(Mo-Se_1)^{inter}$). The other three Se_1 atoms are bonded to the same unit ($(Mo-Se_1)^{intra}$).

This particular arrangement of the Mo_6X_8 units leaves empty vacant channels running along the three rhombohedral axes of the structure where the cations can be inserted. In the case of Chevrel phase based on large cations (e.g., RE), the cations occupy only one of the three possible cavities of the crystal structure site,[14,15] which corresponds to the origin site of the rhombohedral unit cell (Figure 1).

All the characteristic distances are given in Table 4.

(5) Discussion

As indicated above, the presence of rare-earth vacancies in all of our crystals makes a discussion on the influence of the rare-earth ionic radius on the structural parameters much more difficult. These parameters may, in fact, depend on several different factors, and especially on the overall rare-earth concentration. This parameter, through charge-transfer mechanisms from the RE atoms toward the Mo_6 clusters, introduces important structural variations. The charge transfer defines a number of "valence electrons per cluster", called VEC, which depends on the amount of inserted M cations (here rare-earth) and on the oxidation states of these cations. Different studies have shown the influence of the VEC on the cluster's size,[16]

(14) Guillevic, J.; Le Strat, H.; Grandjean, D. *Acta Crystallogr*. **1976**, *B32*, 1342.
(15) Peña, O.; Gougeon, P.; Sergent, M.; Horyn, R. *J. Less-Common Met*. **1984**, *99*, 225.
(16) Yvon, K. In. *Current Topics in Materials Science*; Kaldis, E., Ed.; North-Holland, Amsterdam, 1979; Vol. 3, pp 53−129.

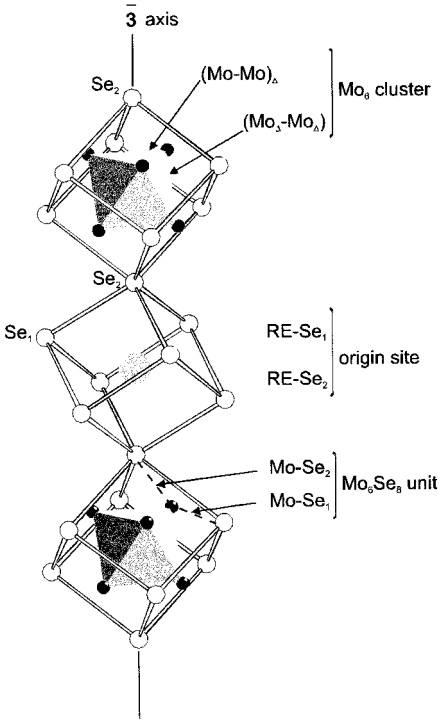

Figure 1. Crystal structure of $RE_xMo_6Se_8$, showing selected interatomic distances.

and we recently reported a full work concerning the variation of the interatomic distances as a function of the VEC number in single crystals of $La_xMo_6Se_8$.[7]

In consequence, to evaluate the influence of the rare-earth ionic radius on the structural parameters of the $REMo_6Se_8$ series, we have to work at a constant VEC number, that is, the rare-earth content should be kept the same, or as similar as possible in all of the $Re_xMo_6Se_8$ crystals under investigation. The systematic presence of RE vacancies in our crystals forced us to choose some average value of x(RE), and consequently, to perform several crystallographic studies for each $REMo_6Se_8$ compound, until we obtained the same approximate stoichiometry for all phases. This average value of x(RE) was chosen to be 0.86−0.87 (**1**, $La_{0.88}Mo_6Se_8$; **3**, $Pr_{0.86}Mo_6Se_8$; **4**, $Nd_{0.85}Mo_6Se_8$; and **5**, $Sm_{0.87}Mo_6Se_8$). The light differences in the values of n—and therefore in the VEC number—are not large enough to lead to significantly different charge-transfer effects.

In the case of the cerium compound, the analyzed crystals yielded quite different stoichiometries from such average values. Two crystals were then chosen, $Ce_{0.82}Mo_6Se_8$ (**2a**) and $Ce_{0.92}Mo_6Se_8$ (**2b**), for which the mean value of x ($x = 0.87$) could be used for comparison. Assuming a linear variation of the interatomic distances with x,[7] we can safely compare the data of both crystals with the rest of the series. Figures 2−6 and Figure 8 show two sets of data for $Ce_xMo_6Se_8$, their average value being the one of a hypothetical $Ce_{0.87}Mo_6Se_8$.

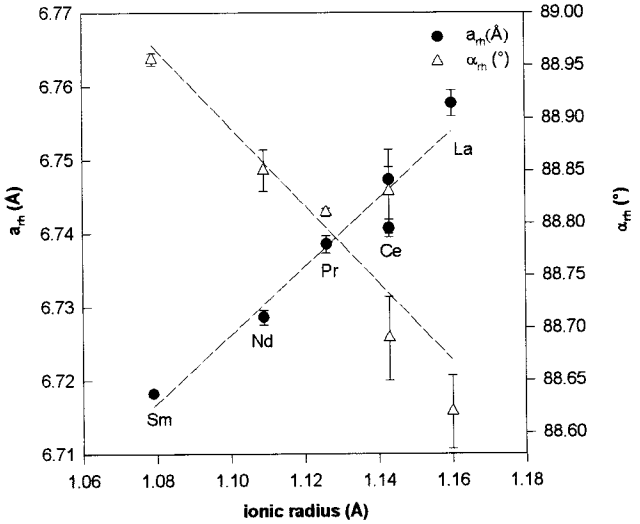

Figure 2. Lattice parameters (a_{rh} and α_{rh}) versus the rare-earth ionic radius for single crystals of $RE_xMo_6Se_8$. The two sets of data for Ce correspond to the experimental values obtained for $x = 0.82$ and 0.92, their average ($x = 0.87$) being compared to the other $Re_{0.87}Mo_6Se_8$ compounds (see text).

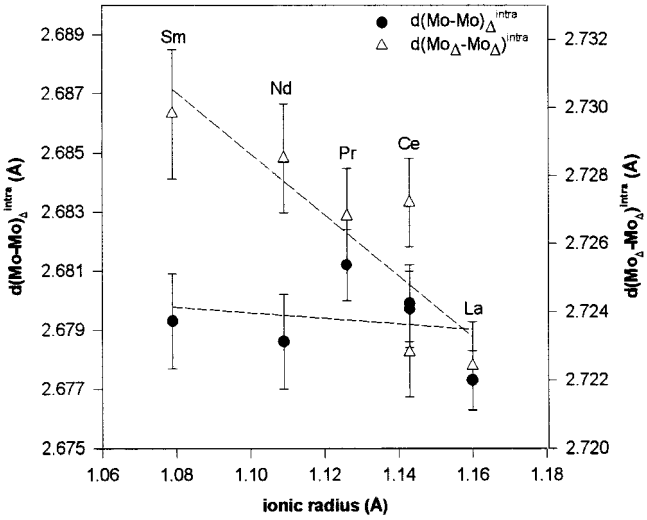

Figure 3. Molybdenum−molybdenum intracluster distances as a function of the RE ionic radius (data for Ce, as defined in Figure 2).

Table 4. Shortest Interatomic Distances (Å) for $RE_xMo_6Se_8$

	1	**2a**	**2b**	**3**	**4**	**5**
compd	$La_{0.88}Mo_6Se_8$	$Ce_{0.82}Mo_6Se_8$	$Ce_{0.92}Mo_6Se_8$	$Pr_{0.86}Mo_6Se_8$	$Nd_{0.85}Mo_6Se_8$	$Sm_{0.87}Mo_6Se_8$
Mo_6 cluster						
$(Mo-Mo)_\Delta^{intra}$	2.6773(4)	2.6797(5)	2.6799(5)	2.6812(6)	2.6786(6)	2.6793(6)
$(Mo_\Delta-Mo_\Delta)^{intra}$	2.7224(5)	2.7272(5)	2.7228(5)	2.7268(7)	2.7285(6)	2.7298(7)
$(Mo-Mo)^{inter}$	3.4400(5)	3.4140(5)	3.4255(5)	3.4090(7)	3.3970(6)	3.3807(7)
Mo_6Se_8 unit						
$(Mo-Se_1)^{intra}$	2.5660(4)	2.5624(6)	2.5644(4)	2.5632(6)	2.5626(6)	2.5618(8)
	2.5721(4)	2.5736(6)	2.5727(4)	2.5740(6)	2.5717(6)	2.5709(7)
	2.6376(4)	2.6390(6)	2.6432(5)	2.6438(6)	2.6428(6)	2.6447(8)
$(Mo-Se_1)^{inter}$	2.7238(4)	2.7142(4)	2.7224(5)	2.7177(6)	2.7142(6)	2.7122(8)
$(Mo-Se_2)$	2.5038(3)	2.5041(4)	2.5052(4)	2.5079(5)	2.5080(5)	2.5093(5)
origin site						
$RE-Se_1$	3.1330(3)	3.1207(5)	3.1176(4)	3.1106(5)	3.1020(5)	3.0892(6)
$RE-Se_2$	2.9014(2)	2.8637(3)	2.8847(4)	2.8595(3)	2.8439(3)	2.8228(4)

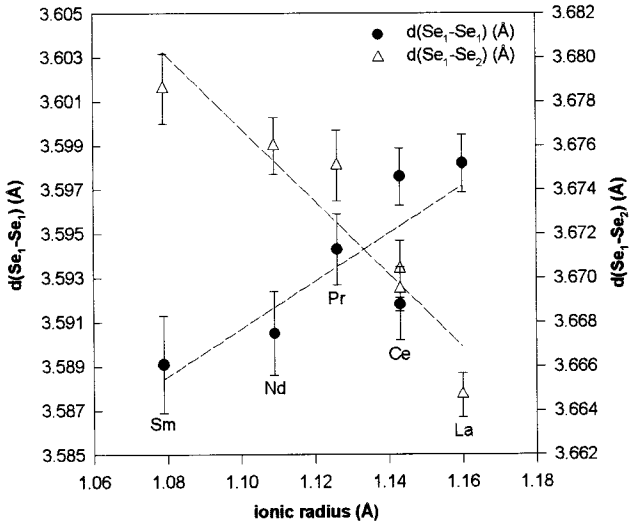

Figure 4. Characteristic interatomic distances of the pseudocube Se_8 circumscribing the Mo_6 cluster versus the RE ionic radius (data for Ce, as defined in Figure 2).

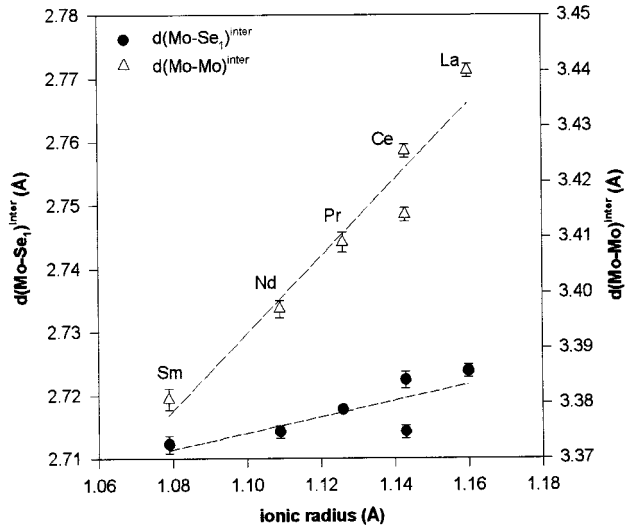

Figure 5. Intercluster distances as a function of the RE ionic radius (data for Ce as defined in Figure 2).

Finally, we should keep in mind that, for all of these compounds, the interatomic distances deduced from the structural refinement correspond, in fact, to the average situation between unit cells at which the origin site is filled (~87%) and those at which the site is empty (~13%). Our discussion will therefore be based on average values.

(5.1)The Cell Parameters versus the Ionic Radius of the Rare-Earth Atom. As expected, the overall lattice volume (V_{rh}) changes linearly with the ionic size of the rare-earth atom (r_i), which is in good agreement with the lanthanide contraction. However, both of the cell parameters (a_{rh} and α_{rh}) vary in opposite directions, one (a_{rh}) increasing proportionally to r_i, the other (α_{rh}) decreasing as the ionic radius increases (Figure 2). The two opposite variations of a_{rh} and α_{rh} show that the insertion of a large rare-earth atom will elongate the unit cell along the $\bar{3}$ axis: as the larger the rare-earth atom, the more elongate the unit cell will become. This cell elongation explains the variation of a_{rh} and V_{rh}.

(5.2) The Interatomic Distances versus the Ionic Radius of the Rare-Earth Atom. Figure 3 shows the influence of the rare-earth ionic radius on the size of the molybdenum cluster. It can immediately be seen that the molybdenum−molybdenum

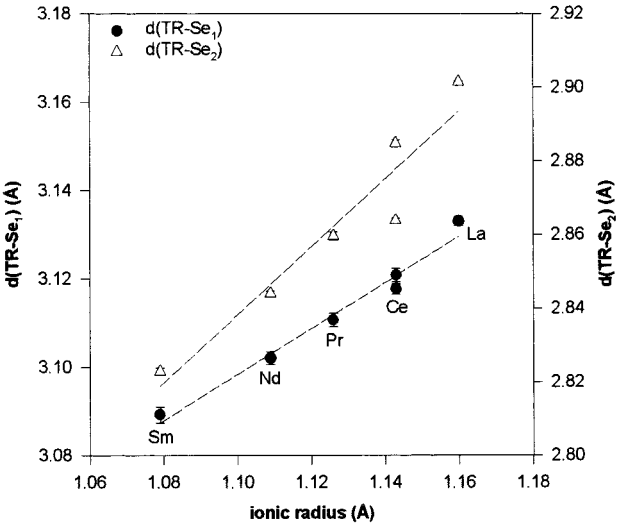

Figure 6. Interatomic distances characterizing the $RESe_8$ pseudocube at the origin site (data for Ce, as defined in Figure 2).

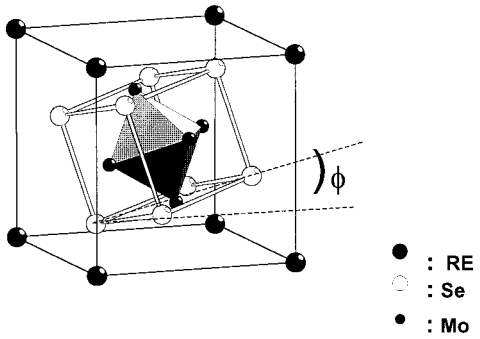

Figure 7. Tilting angle ϕ between the rhombohedral plane and one the faces of the Se_8 pseudocube.

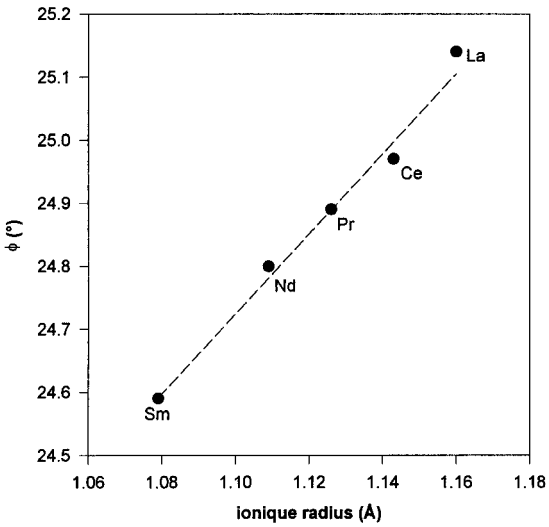

Figure 8. Variation of the tilting angle of the rhombohedral cell around the ternary axis.

intracluster distances behave differently as a function of the rare-earth size. Although the $(Mo-Mo)_{\Delta}^{intra}$ distance remains constant regardless of the rare-earth size, the $(Mo_{\Delta}-Mo_{\Delta})^{intra}$ distance decreases with increases in the radius. Because these two distances define the size and shape of the Mo_6 octahedral cluster, this result means that the cluster becomes less asymmetrical (the $(Mo_{\Delta}-Mo_{\Delta})^{intra}$ distance getting closer to the $(Mo-Mo)_{\Delta}^{intra}$ one) and that the octahedral volume contracts when larger cations are introduced at the origin site. This

contraction also occurs when the VEC increases,[7,16] but in the present case, this is due to the chemical pressure exerted by the rare-earth substituent on the metallic cluster.

The same tendency, to get a more regular shape, is observed in the Se_8 pseudocube of the Mo_6Se_8 unit. Here, the two characteristic intracluster distances are (Se_1-Se_1) and (Se_1-Se_2). The first intracluster distance concerns the distance between two neighboring selenium atoms in the general position of 6*f*, and it increases when the ionic radius of the rare-earth atom grows. The second distance represents the distance between two selenium atoms, one situated on general position and one located on the ternary axis (2*c*), and it decreases as the ionic radius increases (Figure 4). These two opposite variations are nearly comparable, so that the pseudocube volume is not greatly modified. As a consequence, the pseudocube Se_8 (and its associated unit Mo_6Se_8) changes shape and shows the same tendency as the Mo_6 cluster to become less asymmetrical when the rare-earth ionic radius increases. This happens when larger atoms are inserted at the origin site.

The separations between Mo_6Se_8 units can be described through several intercluster distances. However, the most important separations are connected to the strongest (Mo−Mo) and (Mo−Se) bonds that exist between clusters. Figure 5 represents the variation of the $(Mo-Mo)^{inter}$ and $(Mo-Se_1)^{inter}$ distances with the rare-earth ionic radius. The observed increase of these distances confirms the increasing separation between Mo_6Se_8 clusters as the rare-earth radius grows.

Last, but not least, the origin site is directly proportional to the size of the rare-earth ion inserted. The distances, RE−Se, representing this origin site increase continuously from samarium to lanthanum (Figure 6), in good agreement with the evolution of the rare-earth ionic radius with the number of 4f electrons (lanthanide contraction). However, the variation of ($RE-Se_2$) is more important than that of ($RE-Se_1$). As a result, the substitution of a rare-earth ion by a larger one creates not only an increase in the volume of the origin site but also an increase in its elongation along the ternary axis.

Finally, we have determined the tilting angle, Φ, which allows the bonding between two Mo_6Se_8 units. Thanks to this angle, the Se_1 atoms situated at the corners of each unit are immediately facing the Mo atoms of a nearby cluster (cf. Crystal Structure). The angle Φ was calculated for each compound by considering that it corresponds to the angle between a rhombohedral plane and one of the faces of the Se_8 pseudocube, as it is shown in Figure 7. The angular variations depend on the rare-earth atom inserted, the larger its radius, the more important the tilt becomes (Figure 8). It should be noted that Φ does not seem to depend on the RE content because the cerium (and lanthanum[7]) data yielded only one value of Φ for each compound.

(6) Conclusion

In conclusion, the crystallographic study performed on $REMo_6Se_8$ single crystals allowed us to fully characterize the selenide Chevrel phases based on light rare-earth atoms. One of the main results reported here concerns the chemical pressure exerted by the large RE^{3+} ions on the Mo_6Se_8 units. The deformation of the Se_8 pseudocube is inhibited, and the Mo_6 octahedral cluster tends to become symmetrical when the rare-earth ionic radius increases (from Sm to La). The pseudocubic site $RESe_8$ at the origin expands, while slightly elongating along the ternary axis. All intercluster distances increase proportionally to the size of the inserted atom, producing an overall increase of the lattice volume. However, the increase is mainly due to the rhomboedral a_{rh} lattice parameter, whereas the angle α_{rh} decreases. As a result, the crystal elongates along the ternary axis, from $SmMo_6Se_8$ to $LaMo_6Se_8$.

From this study, important conclusions can be drawn concerning the possibility of growing single crystals of $REMo_6Se_8$ phases containing heavy rare-earth atoms. Indeed, extrapolations of the above data to smaller ionic radii (e.g., $r_i(Er^{3+}) = 1.004$ Å, $r_i(Yb^{3+}) = 0.985$ Å)[17] show that the lattice parameters and interatomic distances become close to those of the binary Mo_6Se_8 (e.g., $a_{rh} = 6.654$ Å, $\alpha_{rh} = 91.76°$), and an epitaxial-growth mechanism may be favored.[10]

Acknowledgment. The authors sincerely acknowledge R. Horyn from Wroclaw and M. Sergent and C. Perrin from Rennes for their remarkable help in the early stages of this work and to M. Potel for acquiring all of the data for the crystal structure refinements. This report is realized as a part of a thesis work presented at the University of Rennes, by F. Le Berre (1996) and C. Hamard (1999).

Supporting Information Available: All X-ray crystallographic data is available in simple text format and includes tables of positionnal parameters, bond distances, *B* and *β* factors, RMS, and *U* factors. This material is available free of charge via the Internet at http://pubs.acs.org.

IC990762Z

(17) Shannon, R. D. *Acta Crystallogr*. **1976**, *A32*, 751.
(18) Le Berre, F. Thesis, University of Rennes I, France, 1996.